Synthesis, Structure and Mechanics of Nano-Particulate Aggregates

Carsten Schilde and Arno Kwade

Abstract In the most industrial processes nano-sized particles aggregate during their synthesis and the subsequent drying step forming aggregates with sizes in the order of several micrometers. The properties of these aggregates for application or further processing are specified by particle characteristics such as morphology, size, size distribution, bonding mechanism and structure of primary and secondary particles. In this study, the effect of the process parameters during particle synthesis and the following drying step on the structure formation and the resultant product and processing characteristics of precipitated nano-structured silica aggregates were investigated. For this purpose, the educts concentrations, stabilizing additives, mechanical energy input, pH-value and precipitation temperatures were varied during the precipitation process. In addition to the structure formation during precipitation, the resultant micromechanical aggregate properties of spherical silica model aggregates with a well-defined aggregate structure were characterized via nanoindentation and related to the aggregate structure and the interparticulate interaction forces. The micromechanical properties of these model aggregates were modelled depending on their structure using a modified form of the elementary breaking stress model of Rumpf. Since the characterization of particle-particle interactions in the nanometer size range is hardly possible, this effect on the aggregate fracture and deformation behavior was investigated by simulating the nanoindentation measurement of single aggregates using the "discrete element method".

Keywords Aggregates · Micromechanical properties · Nanoindentation · DEM · Silica · Precipitation

C. Schilde (✉) · A. Kwade
Institute for Particle Technology, TU Braunschweig,
Volkmaroder Str. 5, 38104 Braunschweig, Germany
e-mail: c.schilde@tu-bs.de

M. Kind et al. (eds.), *Colloid Process Engineering*,
DOI 10.1007/978-3-319-15129-8_9

1 Introduction

In the last years, the industrial mass production of nano-particulate products via pyrolysis or precipitation processes which are commonly used in the chemical, pharmaceutical, food and dye industry increases continuously. For these processes, the nano-sized particles typically aggregate during their synthesis and the subsequent drying step to aggregates with sizes on the order of several micrometers. The application of nanoparticle-based products is specified by the characteristics of the nanoparticle's resulting primary and secondary particles (Fig. 1). Thus, morphology, size, size distribution, bonding mechanism, and structure of primary and secondary particles are crucial factors, for determining possible applications [4]. These characteristics depend on the physicochemical properties of the particles as well as on the process parameters during synthesis and the subsequent drying step. Typically, a redispersion is necessary to obtain separately dispersed primary particles or defined aggregate sizes. The influential factors for such a dispersion process can be classified into the formulation of the homogenous phase, the stress mechanisms, intensity and frequency of the dispersing device, and the mechanical aggregate properties generated during particle synthesis [31, 41].

In order to obtain an optimized and economical dispersion process as well as the desired product properties, extensive knowledge of the structure formation during particle synthesis and its effect on the mechanical aggregate properties is necessary. This includes the surface modification, particle-particle interactions, the formation of solid bridges, the porosity, and the size distribution of the primary particles and aggregates. Currently, very little information is available regarding the relationship of the process and formulation parameters of the particle synthesis and the resulting aggregate structure properties on the one hand, and the micromechanical aggregate properties and the dispersion behavior on the other hand. This

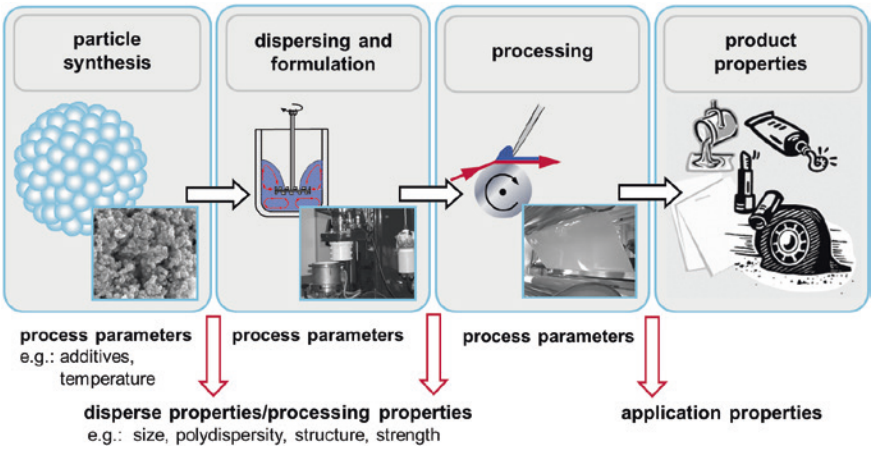

Fig. 1 Effect of process parameters on the processing and application properties

process-structure-property relationship is the main contribution within this study [6, 21, 25–27, 32, 34–39, 42]. Here, we discuss the following questions:

1. How do the process and formulation parameters during particle synthesis affect the primary particle formation, aggregate structure, and solid bridge formation?
2. What is the relationship between the micromechanical properties and the aggregate structure? How does one obtain/receive detailed information about particle interactions, solid bridges, and the behavior of deformation and fracture?
3. Can stress-strain relationships be derived from a series of indentation experiments, e.g. with the help of the discrete elements method?
4. Is it possible to relate micromechanical aggregate properties to application properties such as the dispersion process?

2 Structure Formation During Precipitation

In this project, a semi-batch silica precipitation process from inorganic solvents was investigated. Due to economic reasons and the well-known aspects of this silica synthesis, this process is established for mass production of silica in industrial processes. The precipitation process, especially those of water-soluble silicates are summarized extensively by Hinz [12], Iler [13], and Bergna [7]. By continuously adding sulphuric acid and sodium silicate to a buffer solution of water and sodium silicate, simultaneous primary processes take place. These process include the primary processes such as mixing, reaction and condensation of monomers, phase separation and primary particle growth, as well as the secondary processes such as aggregation, fragmentation, reorganization and aging [15] (see Fig. 2). These physicochemical processes and

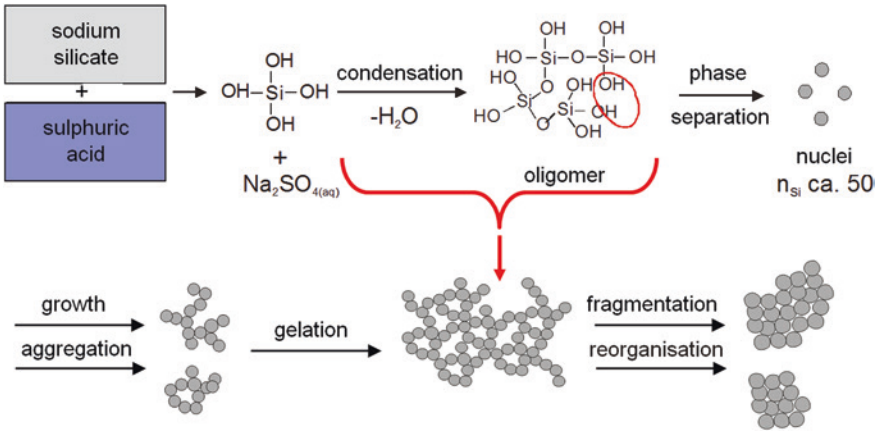

Fig. 2 Primary and secondary processes during silica precipitation process according to Schlomach and Kind [43, 44] (condensation, phase separation, growth and aggregation, gelation, fragmentation and reorganization)

the resultant processing and application properties of the finished product, e.g. the depressibility in further processing, are related to the various formulation and process parameters in a complex way [36]. An extensive investigation of process and formulation parameters of the specific set-up used in this work is given by Schlomach, Kind and Quarch [24, 43, 44]. However, the effect of these parameters on further processing and the micromechanical product characteristics has not been sufficiently investigated until now. Hence, in this project, the effect of formulation parameters, e.g. ion concentration, supersaturation, additives, and process parameters, e.g. precipitation temperature, pH-value, precipitation time, stirrer tip speed, supply of mechanical energy for fragmentation, and flow rate was investigated [30, 36, 37].

Figure 3 illustrates an example of the effect of mechanical energy input by different process units on the precipitated product. The stress mechanism, the stress intensity and stress frequency of the processing unit influence the primary (e.g. mixing

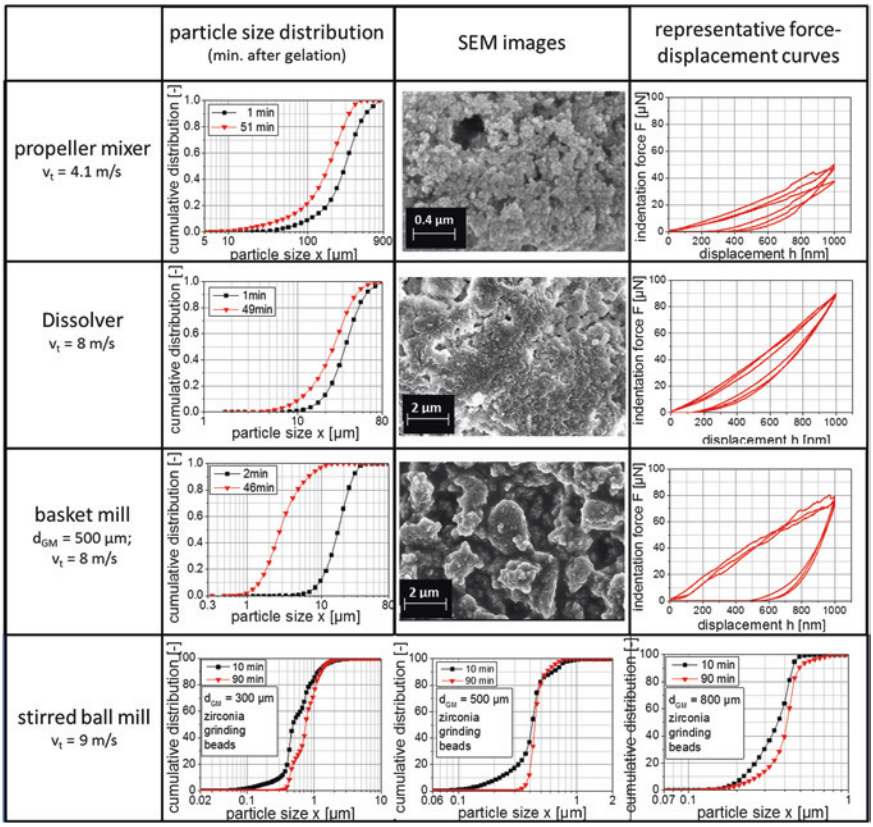

Fig. 3 Effect of mechanical energy input during silica precipitation on the resulting particle size distribution, aggregate structure and mechanical properties (particle size distribution measured via static and dynamic light scattering immediately after the point of gelation and at the end of the precipitation experiment; SEM images of the aggregate structure; representative force-displacement curves measured via nanoindentation)

and reaction of educts, phase separation and primary particle growth) and especially secondary growth and structure formation (e.g. aggregation, fragmentation, reorganization and aging). Typically, precipitation processes are investigated with respect to the mechanical energy input using a stirrer of varying stirrer type or tip speed or T-mixers and ultrasonic homogenizers during various precipitation processes [11, 17, 29, 47, 49]. In this study, the effect of mechanical energy input was investigated for turbulent shear flow using a stirred 4 L tank, equipped with a propeller mixer (Eurostar Euro-ST P CV, company IKA Labortechnik) and a dissolver, which has a process chamber volume of 1 l (toothed lock washer, company Getzmann). Moreover, the compression and shear stress between the surfaces was investigated by integrating a basket mill, which was based on the dissolver set-up (company Getzmann) inside the precipitation reactor, or by using a stirred media mill as precipitation unit (PM1, company Bühler) [30]. Consequently, by using various stirrer and mill types during precipitation, the primary particles and aggregated structures are stressed by different stress mechanisms, stress intensities, and frequencies. For example, in basket mills or stirred media, the stress intensity acting on the aggregates is inversely proportional to the third power of the particle size. Thus, the stress intensity increases strongly with increasing product fineness [18–20, 40]. In contrast, by using stirred precipitation units, the stress intensity is independent of the aggregate size or even decreases with decreasing aggregate size [16].

In case of the semi batch precipitated silica, the concentration and the solubility of monomeric sodium silicate are the crucial factors for the nuclei formation and growth, and not the mechanical energy input. Aggregation, fragmentation and reorganization processes are, however, significantly affected by different stress mechanisms, stress intensities and frequencies during the precipitation process (Fig. 3). Typically, when using a mechanical energy input by turbulent shear flow using stirrers or discs, the aggregate size distribution is shifted to smaller particle sizes and broader particle size distributions with increasing precipitation time after the point of gelation. The higher the mechanical energy input of the stirrer, the more decisive its effect on fragmentation and reorganization processes is. Quarch et al. derived a semi-empiric model for the minimum median aggregate size following the point of gelation [25]. Here, the maximum aggregate fineness is determined as a function of the fluid density and viscosity as well as the power input of the stirrer. Since various stress mechanisms as a function of aggregate size and the stirrer geometry are not considered, this semi-empiric model is not applicable for other dispersing units such as T-mixers, ultrasonic homogenizers, basket mills or stirred media mills. For basket mills and stirred media mills, the effect of the operating parameters on the maximum median aggregate size during precipitation can be described by the frequency of stress events between the grinding media. Thus, according to Schilde et al. [37], the equation for the stress frequency, which depends on the grinding media diameter, grinding media density, tip speed and filling ratio, is applicable for the calculation of the resulting aggregate sizes.

Generally, the higher the mechanical power input the higher the product fineness at the end of the precipitation process. Due to high stress intensities and frequencies between the grinding media, a high product fineness and narrow particle

size distributions are obtained using a stirred media mill as the dispersing unit. The effect of grinding media on aggregate formation and mechanical aggregate properties (see nanoindentation results in Fig. 3) is discussed in more detail by Schilde et al. [37]. In summary, the aggregate size and structure at the end of the silica precipitation process depends on:

- Properties of the fluid phase: Additives, temperature, pH-value, ion concentration, and concentration of precursors
- Properties of the generated gel structure at the point of gelation: Structure, primary, coordination number, porosity, strength of solid bonds or type of particle-particle interactions
- The dispersing unit: Operating parameters, geometry, stress mechanism.

3 Effect of the Aggregate Structure on the Mechanical Properties

In addition to the structure formation during the precipitation process, the relationship between the resultant deformation and fracture behavior, the aggregate structure, and the interparticulate interaction forces was investigated. The effect of the process temperature, the mechanical energy input, various additives to the aggregate structure, and solid bridges formation during the precipitation process as well as the resultant aggregate deformation behavior is described by Schilde [30]. However, since the precipitated silica aggregates are broadly distributed and inhomogeneous in structure, a relationship between specific aggregate structure properties and the deformation and fracture behavior is hardly possible. For this reason, silica model aggregates with different monomodal primary particle sizes between 50 and 400 nm produced from Stöber synthesis (ISC, Würzburg, Germany) were investigated using Tetraalkoxysilane and water as precursors [10, 48]. A narrow aggregate size distribution of homogeneous, spherical aggregates between 5 and 50 µm was obtained by a spray drying process; the classification of aggregates less than 5 µm was acquired using a cyclone (spray dryer, company Büchi). The aggregate structure for a primary particle size of 50 nm is shown in Fig. 4. Due to the spray drying process, a small amount of aggregates contains undesirable void volumes in the aggregate center [51].

The micromechanical properties of the silica aggregates were measured via a displacement controlled deep-sensitive normal force measurement, which used a complete automated nano-mechanical testing system (TriboIndenter® TI 900, company Hysitron Inc.). The silica model aggregates were stressed at a constant loading rate of 100 nm per second (loading and unloading) using a Flat Punch specimen. To guarantee an indentation displacement less than 10 % of the aggregate size which is equivalent to a minimized influence of the substrate, a maximum indentation displacement of 500 nm was chosen. Moreover, the confidence level was increased and the measurement artifacts due to different aggregate sizes were avoided by stressing aggregates in a size range between 10 and 15 micrometers [38, 39]. Further specifications as well as a detailed description

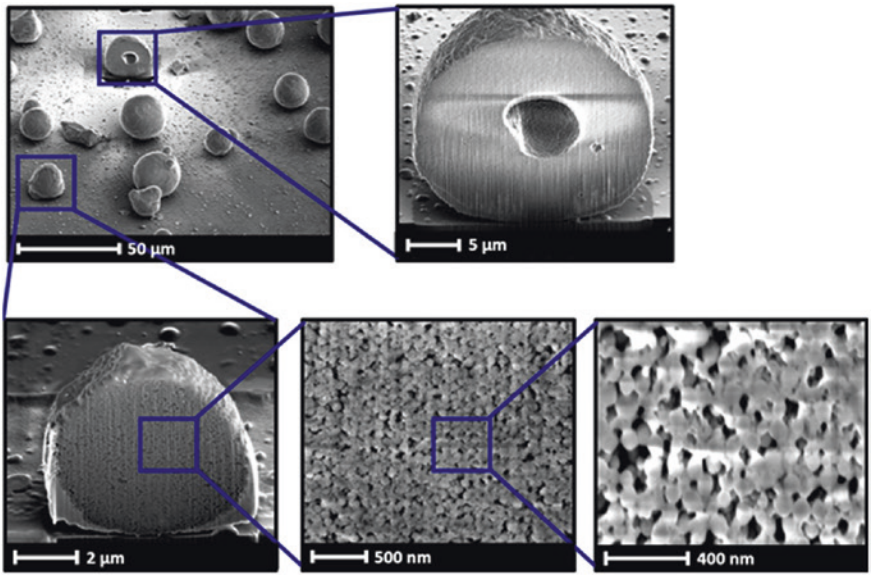

Fig. 4 Combined SEM-FIB images of silica model aggregates with a primary particle size of 50 nm (*top right* aggregate with void volume; *bottom* without void volume)

on the working principle of the nanoindentation device and the sample preparation (precise calibration regarding parallelism between sample and indenter tip and sample preparation via the dry dispersing device RODOS, company Sympatec) are summarized by Schilde [30] and Arfsten [3]. Since the model of Oliver and Pharr (calculation of Young's modulus or hardness) is not applicable for materials with high viscoplastic deformation behavior, the maximum indentation force as well as plastic and elastic deformation energies were determined as characteristics for the micromechanical aggregate properties [36, 39, 42]. Typically, the measurement of these micromechanical properties approached a constant median value as well as a constant standard deviation of approximately 40 single measurements [42].

Figure 5 shows the maximum indentation force and standard deviation as a function of the number of measured silica model aggregates. A constant standard deviation is determined by the inherent distribution of the micromechanical properties of the aggregated system [42]. In contrast to the distribution of the micromechanical properties of individual particles or single crystals, which can be described by Weibull statistics [14, 50], the distributions of aggregates can be described by a log-normal distribution [42]. Consequently, the specification of the log-normal fit can be used for the characterization of the measured system.

In accordance with Schönert and Rumpf [28, 45], an increase in the strength of aggregates and their resistance against fragmentation into smaller sized aggregates was observed with decreasing primary particle size [30]. This effect is due to a reduction of defects within the particulate structure and a smaller decrease in the bonding forces compared to other forces [33]. Figure 6 shows the logarithmic

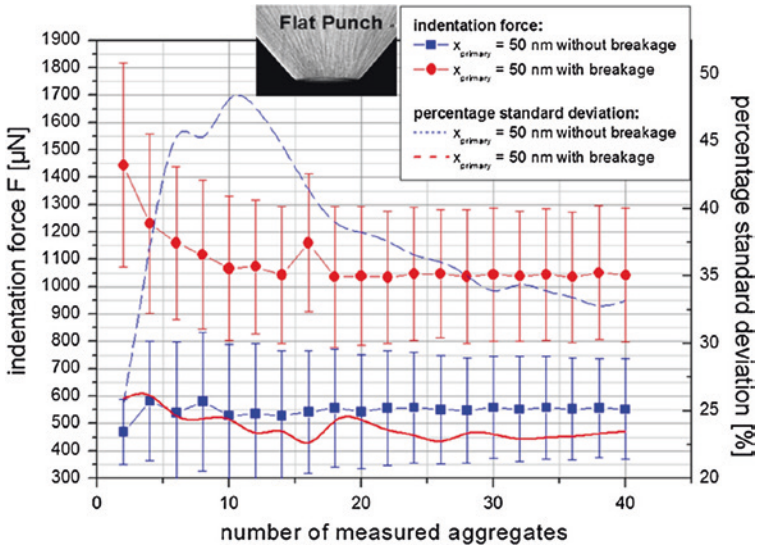

Fig. 5 Maximum indentation force and standard deviation as a function of the number of measured silica model aggregates ($x_{primary} = 50$ nm) using a flat punch indenter geometry [39]

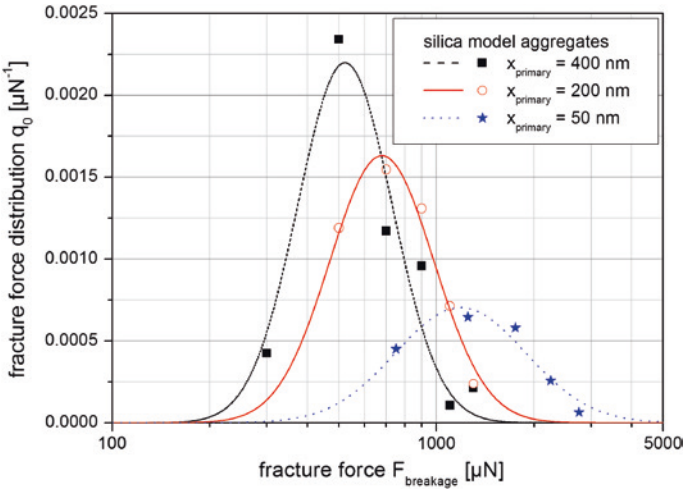

Fig. 6 Logarithmic breakage force distributions of the silica model aggregates with various primary particle sizes [30]

breakage force distributions of the silica model aggregates with various primary particle sizes. At a constant aggregate size, the fracture force increases with decreasing primary particle size. This characteristic micromechanical properties obtained from the load-displacement curves of fractured aggregates can be

Table 1 Aggregate structure properties [39]

Primary particle size $x_{primary}$ (nm)	Porosity ε (−)	Coordination number k(ε) (−)	Solid bridge diameter d_{sb} (nm)
50	0.396	6	30.36
200	0.255	12	84.94
400	0.242	12	163.45

used for the correlation of process properties, e.g. the stress energy distribution obtained from DEM-CFD simulations with dispersion kinetics. First correlation between the fracture force distribution, the stress conditions during stirred media milling and the dispersion results is presented by Schilde et al. [32] and Beinert et al. [5, 6]. Based on the stress energy distribution of the mill, $Q_{0,m}(SE)$, the number of grinding bead contacts per unit time, N_c/t, and the fracture energy distribution of the aggregated system, G3(FE), an effective dispersion fraction, Deff, can be calculated:

$$D_{eff} = \frac{N_c}{t} \cdot \int_{FE_{min}}^{SE_{max}} \left(1 - Q_{0,m}(SE)\right) \cdot G_3(FE) dE \tag{1}$$

Generally, the micromechanical aggregate properties depend on structure characteristics such as primary particle surface, porosity, strength and radius of solid bridges, and coordination number. Based on the structure characteristics in Table 1 (porosity and coordination number determined via mercury porosity, primary particle and solid bridge radius via SEM) and the assumption of isotropic aggregate deformation behavior, the fracture forces for spherical primary and secondary particles can be represented by the concept of the elementary breaking stress according to Rumpf [39]:

$$\sigma_{\text{Rumpf}} = \frac{(1-\varepsilon)}{\Pi} \cdot k(\varepsilon) \cdot \frac{F}{x_{\text{primary}}^2} \tag{2}$$

where ε is the specific void volume of the aggregate, k the average coordination number, π is the mathematical constant Pi, $x_{primary}$ is the primary particle size and F the particle-particle interaction force acting in the particle contacts. Under the assumption of cylindrical solid bridges, the particle-particle interaction force (for tensile, compression or shear stress) can be described as a function of the strength of the solid bridge, σ_{sb}, and the narrowest portion, or neck, of the bridge, r_{sb}, according to the model of Bika et al. [8]:

$$F = \Pi \cdot r_{sb}^2 \cdot \sigma_{sb} \tag{3}$$

For constant strength of the solid bridges, Fig. 7 shows the ratio of the median fracture force and the cross-section area of the aggregates as a function of the structure characteristics according to the Rumpf formula (Eqs. 2 and 3). As

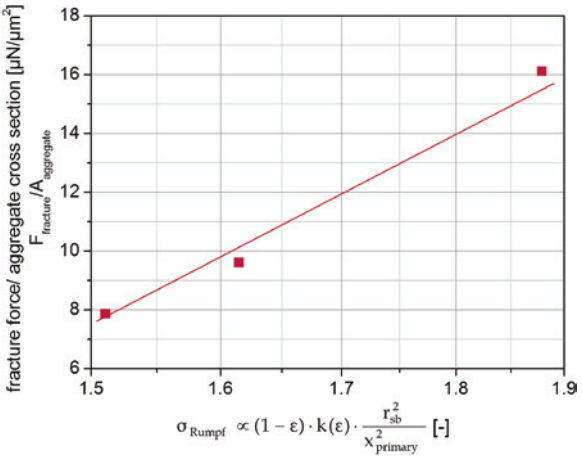

Fig. 7 Median fracture force of the silica model aggregates with various primary particle sizes as function of the elementary breaking stress according to Rumpf (simplified; strength of the solid bridge, σ_{sb}, is assumed constant)

expected, a linear correlation can be obtained. Therefore, the slope of this correlation is a value of the strength of the solid bridges. This relation is valid for the same particle material and, thus, a nearly constant deformation behavior [39].

Since the aggregate structure characteristics such as porosity and coordination number depend strongly on the primary particle morphology, the generalized form of the theory of Rumpf has to be adopted for variations in the primary particle morphology. Thereby, the porosity and coordination number can be characterized as function of the aspect ratio of the primary particles, f_0, which is already described for bulk solids by various authors [9, 52]. An example for the adaption of the generalized model of Rumpf for agglomerates containing primary particles with different morphologies is discussed by Schilde et al. [42]:

$$\sigma_{Rumpf} = (1-\varepsilon) \cdot k \cdot \frac{F_A}{S_p} = c \cdot \phi(f_0) \cdot k(f_0) \cdot \frac{F}{S_p} \tag{4}$$

where φ ($\varphi = 1 - \varepsilon$) is the volume fraction and S_p is the specific particle surface. In principle, the model of Rumpf is applicable in describing the micromechanical aggregate properties for spherical aggregates or agglomerates, constant aggregate diameter, similar deformation behavior and particle-particle interactions, and constant load function during the nanoindentation measurement.

4 DEM Simulation of the Mechanical Aggregate Properties

For application and further aggregate processing, the particle-particle interactions between primary particles are of substantial interest. A characterization of these particle-particle interactions in the nanometer size range and their effect

on the micromechanical aggregate properties is possible only with an increased measurement effort. More detailed information can be obtained by simulating the nanoindentation measurement with the help of the discrete elements method (DEM). The used contact model for the DEM simulation (EDEM 2.3™, company DEM Solutions) during this project was based on a standard Hertz-Mindlin [23] model, a contact model for solid bonds, and an additional attractive van der Waals interaction force. A detailed description of the contact models, dimensioning and aggregate built up is given by Schilde et al. [35]. Depending on the aggregate structure, normal stresses and tensile stresses, fracture may occur during the nanoindentation process. Figure 8 shows force-displacement curves of measured and simulated aggregate compression tests via nanoindentation with and without aggregate fracture (xprimary = 400 nm). As expected for high solid bridge strengths, no fracture occurs and the characteristic values of the deformation energies, relative amount of broken solid bonds, and the maximum indentation force remain constant [35]. The deformation behavior without aggregate fracture obtained from simulation is in qualitatively good agreement to the measured force-displacement curve (without regard to absolute values). Although slight differences can be observed, the used DEM contact model is suitable for the characterization of the stress-strain relationship and particle-particle interaction forces. Since the local structure (defects, coordination number, solid bridge strength and diameter) of the measured aggregates in the simulation differ, the force-displacement curves for fractured aggregates cannot match. To achieve similar force-displacement curves, the 3D-structure of the aggregated system has to be taken into account which is shown for micro sized particles by Roth et al. [26, 27] (via confocal microscopy).

The effect of various contact model parameters on the resultant values of deformation energies, the quotient of plastic and elastic deformation energy, the relative amount of broken solid bonds, as well as the breakage force are given by Schilde

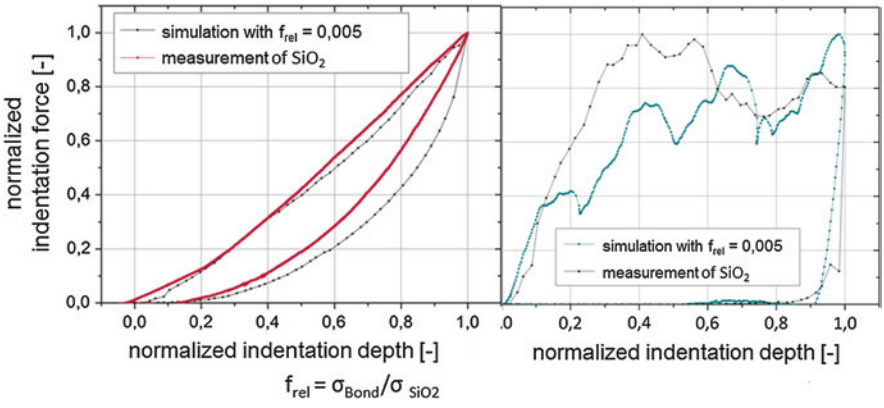

Fig. 8 Force-displacement curves of measured and simulated aggregate compression tests via nanoindentation with (*right*) and without (*left*) aggregate fracture

et al. [35]. Additionally, the load distribution in horizontal direction, which is vertical to the force direction of the indenter, was calculated [35] and compared to the theoretical considerations of Antonyuk et al. [2]. The load distribution provides information on the stresses within the aggregate as well as the deformation behavior [22, 27].

Depending on the particle interactions and the structure, gliding or cleavage cracks occur during the fracture of aggregates (cleavage) or agglomerates (gliding) [1]. Schönert [46] assumed that the highest stress level during impact or compression stress is presented in the area of contact. In the case of aggregates (including solid bridges), these stresses initiate perpendicular to cleavage cracks in the outer radius of the contact region. The cracks are substantially affected by radial stresses between the primary particles. The calculation of the radial stresses based on geometrical aggregate dimensions and forces acting within the solid bridges are described by Schilde et al. [35]. In order to increase the confidential level, the radial forces were averaged over the entire height of the aggregate. Figure 9 illustrates the progression of the absolute values of the radial

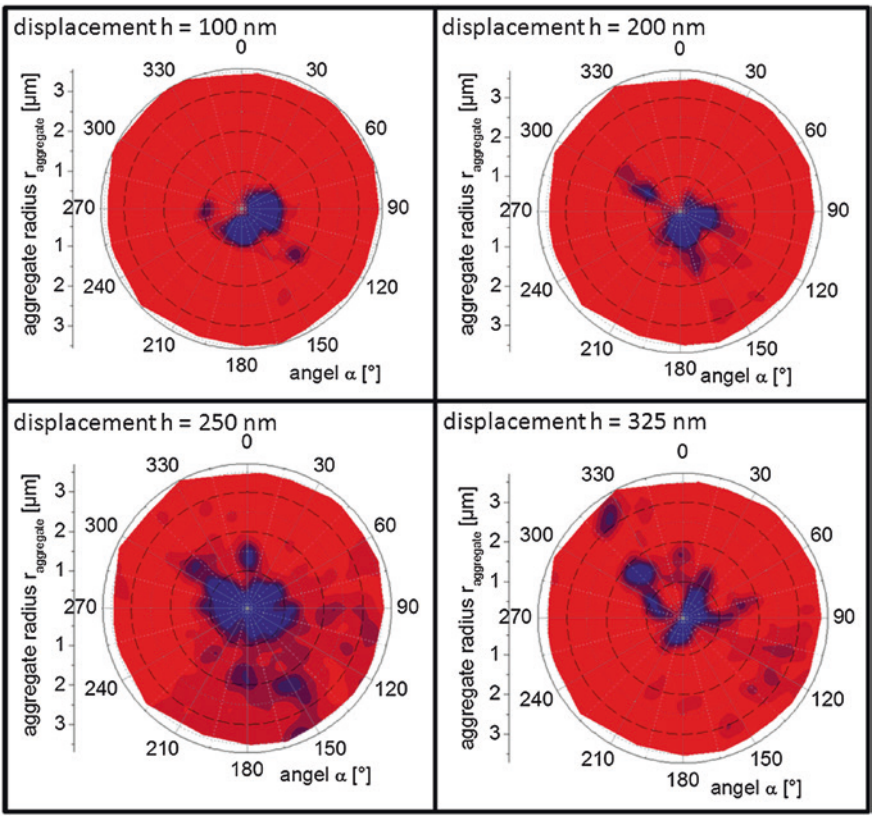

Fig. 9 Distribution of the radial stresses vertical to the force direction of the indenter (x-y section) at different time steps (*dark colors* indicate high radial stresses) [21, 30, 35]

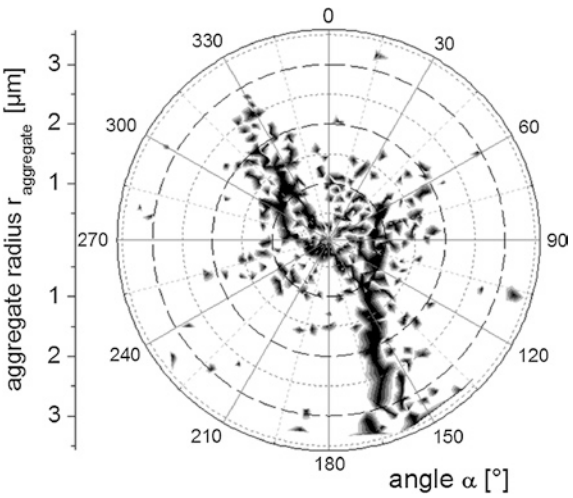

Fig. 10 Solid bonds in case of aggregate fracture (x-y section) (*dark colors* indicate broken solid bonds with acting Van der Waals and Hertz-Mindlin particle-particle interaction forces) [30, 35]; figure by Kwade et al. [21]

stresses at different indentation displacements. As expected, the maximum stresses are located in the area of contact. At a displacement between 200 and 250 nm, the maximum radial stresses are located in the direction of 150° where a first cleavage crack propagates through the entire aggregate (see Fig. 10). At a displacement of 325 nm, a second cleavage crack is induced in the direction of 330° (see Figs. 9 and 10). This is in accordance with the Schönert's conclusions that the radial stresses are responsible for the initiation and propagation of cleavage cracks [46].

5 Conclusion

In summary, it can be stated that the product and processing characteristics of precipitated aggregates are determined by the material itself as well as its structure formation during the particle synthesis. Due to a variation of significant process and formulation parameters, the resulting aggregate structure as well as the micromechanical properties are affected. In the case of particulate systems with plastic or viscoplastic deformation behavior, non-intrinsic characteristics for the characterization of the deformation behavior have to be adopted. In the case of the investigated silica precipitation process, the micromechanical aggregate properties (deformation energies, maximum indentation forces, etc.) can be described by log-normal distributions. With the help of these distributions, the effect of various process and formulation parameters, e.g. additives, educts concentrations, mechanical energy input, pH-value and precipitation temperature, on the structure and solid bridge formation can be described qualitatively. However, the aggregate structure is related to process and formulation parameters of the particle synthesis in a complex way. For this reason, spherical silica

model aggregates with a well-defined aggregate structure were investigated to characterize the effect of the primary particle size, aggregate size, and solid bond strength and stiffness on the micromechanical characteristics. The micromechanical properties of these model aggregates were modelled depending on their structure using a modified form of the elementary breaking stress model of Rumpf. For an isotropic deformation behavior, stresses calculated from the maximum indentation forces and fracture forces can be described by this enhanced model. However, since a characterization of particle-particle interactions between nanoparticles and their effect on the micromechanical aggregate properties is possible only with an increased measurement effort, discrete element simulations were carried out. A combination of a Hertz-Mindlin contact model, a solid bridge model and a model for Van der Waals attraction is suitable to describe the stress-strain-relationship and particle-particle interactions, of nanostructured aggregates. Moreover, the radial stresses acting between primary particles can be correlated to the formation and propagation of cleavage cracks according to Schönert's theoretical considerations.

Generally, the aggregate structure and its effect on their micromechanical properties was investigated and combined with the stress conditions during the dispersion process. Certainly, the process-structure-property-relationship cannot be determined completely and was only represented exemplarily in this project.

Acknowledgements The authors gratefully acknowledge the financial support by the DFG within the SPP 1273 "colloid technology". The FIB-SEM pictures were kindly taken by Michael Kappl (MPI, Mainz). Many thanks for the support in the surface functionalization of model silica aggregates and addition of additives during precipitation to Sabrina Zellmer (Institute for Particle Technology, Braunschweig).

References

1. Antonyuk S (2006) Deformations-und Bruchverhalten von kugelförmigen Granulaten bei Druck- und Stoßbeanspruchung. Otto-von-Guericke-Universität Magdeburg, Magdeburg
2. Antonyuk S, Tomas J, Heinrich S, Mörl L (2005) Breakage behaviour of spherical granulates by compression. Chem Eng Sci 60:4031–4044
3. Arfsten J (2009) Mikromechanische Charakterisierung von Saccharomyces cerevisiae. TU Braunschweig, Braunschweig
4. Barth N, Schilde C, Kwade A (2014) Influence of electrostatic particle interactions on the properties of particulate coatings of titanium dioxide. J Colloid Interface Sci 420:80–87
5. Beinert S, Schilde C, Gronau G, Kwade A (2014) CFD-discrete element method simulations combined with compression experiments to characterize stirred-media mills. Chem Eng Technol 37:770–778
6. Beinert S, Schilde C, Kwade A (2012) Simulation of stress energy and grinding media movement within a wet operated annular gap mill using the discrete element method. Chem Eng Technol 35:1899–2059
7. BERGNA HE (1994) The colloid chemistry of silica. American Chemical Society, Washington, DC
8. Bika D, Tardos GI, Panmai S, Farber L, Michaels J (2005) Strength and morphology of solid bridges in dry granules of pharmaceutical powders. Powder Technol 150:104–116

9. Donev A, Cisse I, Sachs D, Variano EA, Stillinger FH, Connelly R, Torquato S, Chaikin PM (2004) Improving the density of jammed disordered packings using ellipsoids. Science 303:990–993
10. Gellermann C, Ballweg T, Wolter H (2007) Herstellung von funktionalisierten oxidischen nano-und mikropartikeln und deren verwendung. Chem Ing Tech 79:233–240
11. Gradl J, Schwarzer H-C, Schwertfirm F, Manhart M, Peukert W (2006) Precipitation of nanoparticles in a T-mixer: coupling the particle population dynamics with hydrodynamics through direct numerical simulation. Chem Eng Process 45:908–916
12. Hinz W (1971) Grundlagen der Silikatwissenschaft und Silikattechnik. Verlag Bauwesen, Berlin
13. Iler RK (1979) The chemestry of silica. Wiley, New York
14. Kendall K (1988) Agglomerate strength. Powder Metall 31:28–31
15. Kind M (2002) Colloidal aspects of precipitation processes. Chem Eng Sci 57:4287–4293
16. Kolmogorov AN (1958) Die lokale Struktur der Turbulenz in einer inkompressiblen zähen Flüssigkeit bei sehr großen Reynoldsschen Zahlen. Sammelband zur statistischen Theorie der Turbulenz, Akademie Verlag Berlin
17. Kucher M, Babic D, Kind M (2006) Precipitation of barium sulfate: experimental investigation about the influence of supersaturation and free lattice ion ratio on particle formation. Chem Eng Process 45:900–907
18. Kwade A (2001) Physical model to describe and select comminution and dispersion processes. Chem Ing Tech 73:703
19. Kwade A (2003) A stressing model for the description and optimization of grinding processes. Chem Eng Technol 26:199–205
20. Kwade A, Kampen I, Breitung-Faes S, Schilde C (2009) Basic course—grinding and dispersing with stirred media mills. Arno Kwade, Braunschweig
21. Kwade A, Schilde C, Burmeister CF, Roth M, Lellig P, Auerhammer GK (2013) Micromechanical properties of colloidal structures. Powders and Grains 1542:939–942
22. Malzbender J, de Witt G (2002) Indentation load-displacement curve, plastic deformation, and energy. J Mater Res 17:502–511
23. Mindlin RD (1949) Compliance of elastic bodies in contact. J Appl Mech 16:259–268
24. Quarch K (2010) Produktgestaltung an kolloidalen agglomeraten und gelen. Karlsruher Institute of Technology, Karlsruhe
25. Quarch K, Durand E, Schilde C, Kwade A, Kind M (2010) Mechanical fragmentation of precipitated silica aggregates. Chem Eng Res Des 88:1639–1647
26. Roth M, Schilde C, Lellig P, Kwade A, Auerhammer GK (2012) Colloidal aggregates tested via nanoindentation and quasi-simultaneous 3D imaging. The Eur Phys J E 35:1–12
27. Roth M, Schilde C, Lellig P, Kwade A, Auerhammer GK (2012) Simultaneous nanoindentation and 3D imaging on semi-crystalline colloidal films. Chem Lett 41:1110–1112
28. Rumpf H (1958) Grundlagen und methoden des granulierens. Chem Ing Tech 30:144–158
29. Saeki T, Ishida M (2011) Production of acid silica sols and gels by using a Y-shaped reactor and dilution technique. Int J Chem Reactor Eng 9:1–11
30. Schilde C (2013) Structure, mechanics and fracture of nanoparticulate aggregates. TU Braunschweig, Braunschweig
31. Schilde C, Arlt C, Kwade A (2009) Einfluss des dispergierprozesses bei der herstellung nanopartikelverstärkter verbundwerkstoffe. Chem Ing Tech 81:775–783
32. Schilde C, Beinert S, Kwade A (2011) Comparison of the micromechanical aggregate properties of nanostructured aggregates with the stress conditions during stirred media milling. Chem Eng Sci 66:4943–4952
33. Schilde C, Breitung-Faes S, Kwade A (2007) Dispersing and grinding of alumina nano particles by different stress mechanisms. Ceram Forum Int 84:12–17
34. Schilde C, Breitung-Faes S, Kwade A (2013) Grinding kinetics of nano-sized particles for different electrostatical stabilizing acids in a stirred media mill. Powder Technol 235:1008–1016

35. Schilde C, Burmeister CF, Kwade A (2014) Measurement and simulation of micromechanical properties of nanostructured aggregates via nanoindentation and DEM-simulation. Powder Technol 259:1–13
36. Schilde C, Gothsch T, Quarch K, Kind M, Kwade A (2009) Effect of important process parameters on the redispersion process and the micromechanical properties of precipitated silica. Chem Eng Technol 32:1078–1087
37. Schilde C, Hanisch C, Naumann D, Beierle T, Kwade A (2013) A novel way to vary the structure of precipitated silica and calcium carbonate aggregates in a wide range by using grinding media during the precipitation process. Chem Eng Sci 94:127–137
38. Schilde C, Kampen I, Kwade A (2010) Dispersion kinetics of nano-sized particles for different dispersing machines. Chem Eng Sci 65:3518–3527
39. Schilde C, Kwade A (2012) Measurement of the micromechanical properties of nanostructured aggregates via nanoindentation. J Mater Res 27:672–684
40. Schilde C, Mages-Sauter C, Kwade A, Schuchman HP (2011) Efficiency of different dispersing devices for dispersing nanosized silica and alumina. Powder Technol 207:353–361
41. Schilde C, Nolte H, Arlt C, Kwade A (2010) Effect of fluid-particle-interactions on dispersing nano-particles in epoxy resins using stirred-media-mills and three-roll-mills. Compos Sci Technol 70:657–663
42. Schilde C, Westphal B, Kwade A (2012) Effect of primary particle morphology on the micromechanical properties of nanostructured alumina agglomerates. J Nanopart Res 14:1–11
43. Schlomach J (2005) Feststoffbildung bei technischen Fällprozessen. Universität Karlsruhe, Karlsruhe
44. Schlomach J, Kind M (2004) Investigations on the semi-batch precipitation of silica. J Colloid Interface Sci 277:316–326
45. Schönert K (1991) Advances of communication fundamentals and impacts on technology. Aufbereitungstechnik 32:487–494
46. Schönert K (2004) Breakage of spheres and circular discs. Powder Technol 143–144:2–18
47. Schwarzer H-C, Peukert W (2004) Combined experimental/numerical study on the precipitation of nanoparticles. AIChE J 50:3234–3247
48. Stöber W, Fink A, Bohn E (1968) Controlled growth of monodisperse silica spheres in the micron size range. J Colloid Interface Sci 26:62–69
49. Tung H-H, Wang L, Panmai S, Riebe M (2009) Nanoparticle formation via rapid precipitation. Patent US20110053927 A1, EP2273978A1, WO2009131930A1
50. Vogel L, Peukert W (2005) From single particle impact behaviour to modelling of impact mills. Chem Eng Sci 60:5164–5176
51. Walker WJ Jr, Reed JS (1999) Influence of slurry parameters on the characteristics of spray-dried granules. J Am Ceram Soc 82:1711–1719
52. Williams SR, Philipse A (2003) Random packing of spheres and spherocylinders simulated by mechanical contraction. Phys Rev E 67:1–9